Equation of state and Helmholtz energy functional for fused heterosegmented hard chains

Philipp Rehner [1,2,*] Thijs van Westen [2] and Joachim Gross [2,†]

[1] *Energy and Process Systems Engineering, Department of Mechanical and Process Engineering, ETH Zurich, Tannenstrasse 3, 8092 Zurich, Switzerland*

[2] *Institute of Thermodynamics and Thermal Process Engineering, University of Stuttgart, Pfaffenwaldring 9, 70569 Stuttgart, Germany*

(Received 23 December 2021; accepted 18 February 2022; published 7 March 2022)

Modern equations of state for real nonspherical molecules are often based on Wertheim's first-order thermodynamic perturbation theory (TPT1). A major drawback of TPT1 is that it assumes tangentially bonded spheres. In this work, we develop a Helmholtz energy functional for systems comprising hard heterosegmented chains with arbitrary bond lengths. This is achieved by using hard-sphere fragments (i.e., hard spheres with spherical caps removed at the intersection to their neighbors) as monomers as opposed to full hard spheres. The model is written as a Helmholtz energy functional for inhomogeneous systems and the equation of state for a homogeneous system is determined as a special case. We thereby obtain an equation of state that can be used as a reference to develop statistical associating fluid theory models that more accurately describe the thermodynamic properties of nonspherical molecules. The model is validated against molecular simulation results of bulk pressures and density profiles in slit pores. For the bulk pressures, we show that the equation of state is in excellent agreement with results from molecular simulation for dimers, trimers, and chains of up to 20 segments. The density profiles of individual segments of the chains are regarded in slit pores. Some deviations of the theory from results of molecular simulations are observed for strongly fused chains. Overall, however, good agreement is found for inhomogeneous systems.

DOI: 10.1103/PhysRevE.105.034110

I. INTRODUCTION

Perturbation theories are powerful tools for the development of accurate models that can describe the fluid-phase properties of real components based on molecular properties. As a prerequisite for the application of a perturbation theory, a reference fluid with well-known properties and preferably no fluid-fluid phase transition has to be defined. Reference fluids of purely repulsive molecules, such as hard spheres or chains of hard spheres, have proven particularly useful in that respect. The description of strongly elongated or chain-like molecules, is commonly done using the first-order thermodynamic perturbation theory (TPT1) by Wertheim [1–4]. A detailed review of Wertheim's theory has recently been published [5]. The combination of Wertheim's perturbation theory for chain formation and a perturbation theory for describing the attractive intermolecular interactions lead to equation-of-state models referred to as statistical associating fluid theory (SAFT) [6]. There are two versions of SAFT, depending on which perturbation theory is applied first. Traditional SAFT models (e.g., SAFT-VR [7], soft-SAFT [8], and SAFT-VR-Mie [9]) treat the effect of the attractive interactions at the level of the monomeric fluid, and subsequently use Wertheim's theory to account for the bonding of these monomers to chains. The PC-SAFT model [10] first applies Wertheim's theory, at the level of the repulsive reference fluid, and then applies a perturbation theory to describe the attractive interactions between chains.

Common for all SAFT versions is that the underlying TPT1 is a model for chains of tangentially bonded spheres. This is in conflict with the molecular understanding and force fields used in molecular simulations, which indicate a significant overlap between the repulsive parts of the potentials of neighboring interaction sites. In molecular equations of state like PC-SAFT this is compensated by allowing the chain-length parameters from TPT1 to have noninteger values. When these parameters are fitted to experimental data, they tend to attain values lower than the actual number of segments in the molecule, which can be interpreted as a measure for the discrepancy between the molecular model assumed by the equation of state for tangent-sphere chains and the geometry of the actual molecule. For (heterosegmented) group contribution methods, in which the number of segments is based on to the actual number of functional groups within the molecules, this disparity needs to be resolved. In the heterosegmented group contribution method for the PC-SAFT equation of state [11,12], properties of individual segments are scaled with the parameter m_α, representing a fraction of a spherical segment. In practice, this parameters tends to attain values smaller than unity to obtain physically meaningful packing fractions. In the SAFT-γ-Mie group contribution equation of state [13] the corresponding parameter is referred to as shape factor S_k. To incorporate the actual shape of the molecules more rigorously in a SAFT equation of state, a fused-sphere chain reference model is required.

*prehner@ethz.ch
†gross@itt.uni-stuttgart.de

Models for fused dimers (so-called hard dumbbells) and fused chains were proposed already before Wertheim's groundbreaking work. Earlier models were based on perturbation theories following the blip-function approach [14] or the reference average Mayer function theory [15,16]. An empirical equation, fitted to results of Monte Carlo simulations was proposed by Tildesley and Streett [17]. In a series of publications, Boublík presents models for dumbbells and fused chains within the framework of scaled particle theory [18,19], later in combination with a chain contribution from TPT1 [20,21]. Based on the success of TPT1 as a core ingredient of the family of SAFT equations of state, more attempts at extending the approach to fused chains were published [22–26]. Generally speaking, reasonable results are obtained, but for strongly fused chains the model predictions deteriorate. Exceptions exist, but those theories are either difficult to apply to chains longer than dimers [26] or require Monte Carlo simulations to generate certain model inputs [22].

In the meantime Helmholtz energy functionals for hard bodies were developed. The functionals are used in classical density functional theory (DFT) [27] to model the properties of inhomogeneous systems like fluids in confined media. A major breakthrough was the fundamental measure theory (FMT) by Rosenfeld [28], that allows an accurate description of hard-sphere mixtures. For bulk systems, the original FMT by Rosenfeld simplifies to Wertheim's solution of the Percus-Yevick integral equation [29]. To improve the description of the bulk limit, Roth *et al.* [30] and Yu and Wu [31] simultaneously published a modified fundamental measure theory that reduces to the Boublík-Mansoori-Carnahan-Starling-Leland (BMCSL) [32,33] equation of state for hard-sphere mixtures for bulk systems. This equation of state is typically used as the hard-sphere reference contribution in equation-of-state models such as SAFT. Rosenfeld later generalized his theory to general convex bodies [34] but the model showed shortcomings in the description of nematic phases, that were later alleviated by Hansen-Goos and Mecke [35,36]. That approach was applied to model the position and orientation of hard dumbbells in confinement by Marechal *et al.* [37]. A generalization of the theory to longer chains is challenging due to the increasing number of orientational degrees of freedom of the chains. Instead, for chains of tangentially bonded spheres, Jain *et al.* [38] use the inhomogeneous version of Wertheim's TPT1 [39] to model the density distribution of individual segments. Our work is a generalization of this modeling approach to fused chain molecules.

We present a Helmholtz energy functional for linear or branched chains of fused, arbitrarily sized hard spheres. The simplification to a heterosegmented group contribution equation of state and further to a simple equation of state for homosegmented chains are shown explicitly because such models can be useful in the context of perturbation theories. The model is compared to simulation results for homogeneous and heterogeneous systems.

II. MODEL

The molecular model considered in this study consists of chains of arbitrarily sized, fused spheres (Fig. 1). The chain is characterized by the individual segment diameters σ_α and the bond lengths $l_{\alpha\alpha'}$. The index α runs over all segments (not necessarily belonging to the same molecule) in the system. Since the chains are flexible, the segments can form arbitrary bond angles, as long as the overlap of nonneighboring segments is entirely contained inside the segments in between.

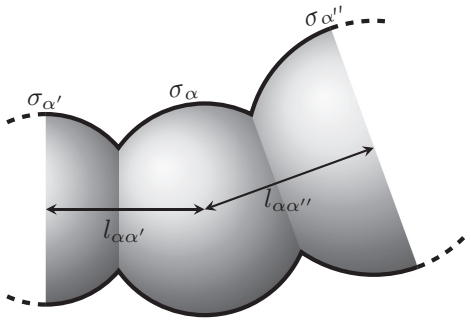

FIG. 1. Geometry of a segment on a chain and its neighboring segments.

A. Fragmented sphere reference fluid

To describe a system of fused chain molecules using the framework of Wertheim's TPT1 [1,2], the chain is cut into spherical fragments, as shown in Fig. 2. The system of hard spherical fragments then defines the reference fluid.

In the limit of tangent-sphere chains, the reference fluid of spherical fragments reduces to a normal hard-sphere reference fluid, which is accurately described by the fundamental measure theory (FMT) as proposed by Rosenfeld [28] and further developed by Roth *et al.* [30] and Yu and Wu [31]. Therefore, it is advisable to devise a model, that recovers the FMT in the limit of no fusing.

In FMT, the Helmholtz energy density [30,31]

$$\beta f^{\text{mono}} = -n_0 \ln(1-n_3) + \frac{n_1 n_2 - \vec{n}_1 \cdot \vec{n}_2}{1-n_3} + \left(n_2^3 - 3 n_2 \vec{n}_2 \cdot \vec{n}_2\right) \frac{n_3 + (1-n_3)^2 \ln(1-n_3)}{36\pi n_3^2 (1-n_3)^2} \tag{1}$$

is given as a function of four scalar and two vector weighted densities $n_k(\mathbf{r})$ and $\vec{n}_k(\mathbf{r})$. These weighted densities are

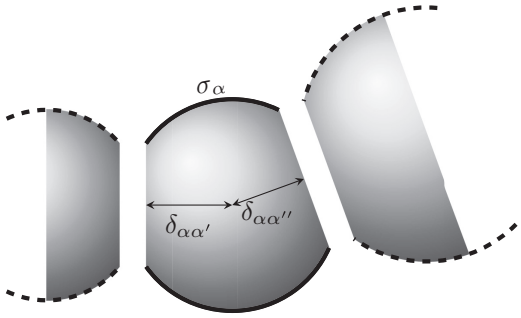

FIG. 2. The volume and surface area of a single segment on the chain are determined from the geometry of the spherical fragment obtained by removing the spherical caps that overlap with neighboring segments.

obtained by convolving the density profiles $\rho_\alpha(\mathbf{r})$ of segment α with the corresponding weight function $\omega_k^\alpha(\mathbf{r})$, as

$$n_k(\mathbf{r}) = \sum_\alpha \int \rho_\alpha(\mathbf{r}')\omega_k^\alpha(\mathbf{r}-\mathbf{r}')d\mathbf{r}'. \tag{2}$$

In FMT, the four scalar weight functions correspond to the so-called fundamental measures of the monomer [40]: the volume ($k=3$), the surface area ($k=2$), the mean radius of curvature ($k=1$), and the Euler characteristic ($k=0$). Therefore, we scale the weight functions according to the fundamental measures of the hard-sphere fragments, defined in Fig. 2. The volume of segment α is

$$V_\alpha = \frac{\pi}{6}\sigma_\alpha^3 - \frac{\pi}{12}\sum_{\alpha'}(\sigma_\alpha - 2\delta_{\alpha\alpha'})^2(\sigma_\alpha + \delta_{\alpha\alpha'}), \tag{3}$$

where the index α' runs over all neighboring segments of α and $\delta_{\alpha\alpha'}$ is that part of the distance $l_{\alpha\alpha'}$ that lays inside segment α as shown in Fig. 2:

$$\delta_{\alpha\alpha'} = \frac{\sigma_\alpha^2 - \sigma_{\alpha'}^2 + 4l_{\alpha\alpha'}^2}{8l_{\alpha\alpha'}}. \tag{4}$$

The weight function ω_3^α is modified as

$$\omega_3^\alpha(\mathbf{r}) = V_\alpha^*\Theta\left(\frac{\sigma_\alpha}{2} - |\mathbf{r}|\right), \tag{5}$$

with the Heaviside step function $\Theta(x)$ and V_α^* defined as the ratio of the volume of the hard-sphere fragment and the volume of the full hard sphere with diameter σ_α, as

$$V_\alpha^* = 1 - \frac{1}{2}\sum_{\alpha'}\left[1 - 3\frac{\delta_{\alpha\alpha'}}{\sigma_\alpha} + 4\left(\frac{\delta_{\alpha\alpha'}}{\sigma_\alpha}\right)^3\right]. \tag{6}$$

For the surface area A_α, only the area of a hard-sphere fragment that does not overlap with adjacent segments is considered, leading to

$$A_\alpha = \pi\sigma_\alpha^2 - \frac{\pi}{2}\sum_{\alpha'}\sigma_\alpha(\sigma_\alpha - 2\delta_{\alpha\alpha'}) \tag{7}$$

and the ratio of the surface of the hard-sphere fragment and the full sphere

$$A_\alpha^* = 1 - \frac{1}{2}\sum_{\alpha'}\left(1 - 2\frac{\delta_{\alpha\alpha'}}{\sigma_\alpha}\right). \tag{8}$$

The corresponding weight function ω_2^α is thus

$$\omega_2^\alpha(\mathbf{r}) = A_\alpha^*\delta\left(\frac{\sigma_\alpha}{2} - |\mathbf{r}|\right), \tag{9}$$

with the Dirac δ function $\delta(x)$. For the radius of curvature, only the spherical parts of the surface have a contribution which is equal to the radius of curvature of the full sphere. The correction factor is thus equal to the correction factor for the surface area. The Euler characteristic is not changed by the fusion, as for each edge a new face is added that cancels it out. The final two scalar weight functions are thus

$$\omega_1^\alpha(\mathbf{r}) = \frac{A_\alpha^*}{2\pi\sigma_\alpha}\delta\left(\frac{\sigma_\alpha}{2} - |\mathbf{r}|\right) \tag{10}$$

and

$$\omega_0^\alpha(\mathbf{r}) = \frac{1}{\pi\sigma_\alpha^2}\delta\left(\frac{\sigma_\alpha}{2} - |\mathbf{r}|\right). \tag{11}$$

The vector weighted densities defined by Rosenfeld [28] cannot be adjusted in a similar manner as the scalar weighted densities because they are equal to zero for a homogeneous system. To choose an appropriate scaling factor, we propose the same relations as used in the FMT for hard spheres, $\vec{\omega}_2^\alpha(\mathbf{r}) = -\nabla\omega_3^\alpha(\mathbf{r})$ and $\vec{\omega}_1^\alpha(\mathbf{r}) = \frac{\vec{\omega}_2^\alpha(\mathbf{r})}{2\pi\sigma_\alpha}$, leading to

$$\vec{\omega}_2^\alpha(\mathbf{r}) = V_\alpha^*\frac{\mathbf{r}}{|\mathbf{r}|}\delta\left(\frac{\sigma_\alpha}{2} - |\mathbf{r}|\right), \tag{12}$$

$$\vec{\omega}_1^\alpha(\mathbf{r}) = \frac{V_\alpha^*}{2\pi\sigma_\alpha}\frac{\mathbf{r}}{|\mathbf{r}|}\delta\left(\frac{\sigma_\alpha}{2} - |\mathbf{r}|\right). \tag{13}$$

B. Chain functional

The development of the chain functional for heterosegmented fused chains follows previous work by Jain *et al.* [38] and Rehner *et al.* [41] which is based on the application of Wertheim's thermodynamic perturbation theory [1–4] to inhomogeneous systems of tangent-sphere chains. For fused chains, the model needs to be modified accordingly.

First, we define a chain contribution

$$\beta f^{\text{chain}} = -\frac{1}{2}\sum_\alpha\sum_{\alpha'}\rho_\alpha \ln y_{\alpha\alpha'}, \tag{14}$$

where the index α' sums over all segments bonded to segment α and $y_{\alpha\alpha'}$ is an effective cavity correlation function. For tangent-sphere chains, $y_{\alpha\alpha'}$ denotes the cavity-correlation function of two hard spheres at contact, which in SAFT equations of state, is usually modeled based on the expression following from the BMCSL equation of state [6,10,32]. Here we apply the BMCSL model to fused chains by replacing the diameters σ_α and $\sigma_{\alpha'}$ with $l_{\alpha\alpha'} + \frac{\sigma_\alpha - \sigma_{\alpha'}}{2}$ and $l_{\alpha\alpha'} + \frac{\sigma_{\alpha'} - \sigma_\alpha}{2}$, respectively. With these expressions, the correct limits for tangent spheres and for entirely fused spheres are obtained (see Secs. II C 2, and II C 3). The expression for $y_{\alpha\alpha'}$ can then be written compactly as

$$y_{\alpha\alpha'} = \frac{1}{1-\zeta_3} + \frac{3b_{\alpha\alpha'}\zeta_2}{2(1-\zeta_3)^2} + \frac{(b_{\alpha\alpha'}\zeta_2)^2}{2(1-\zeta_3)^3}, \tag{15}$$

with

$$b_{\alpha\alpha'} = \frac{4l_{\alpha\alpha'}^2 - (\sigma_\alpha - \sigma_{\alpha'})^2}{4l_{\alpha\alpha'}}. \tag{16}$$

The shape of the hard-sphere fragments is accounted for in the weighted densities ζ_2 and ζ_3. These are calculated analogously to the weighted densities in fundamental measure theory [Eq. (2)], using the weight functions [42]

$$\omega_{\zeta_2}^\alpha(\mathbf{r}) = \frac{A_\alpha^*}{8\sigma_\alpha}\Theta(\sigma_\alpha - |\mathbf{r}|), \tag{17}$$

$$\omega_{\zeta_3}^\alpha(\mathbf{r}) = \frac{V_\alpha^*}{8}\Theta(\sigma_\alpha - |\mathbf{r}|). \tag{18}$$

The monomer and chain contributions define the residual Helmholtz energy, according to

$$F^{\text{res}} = \int [f^{\text{mono}}(\mathbf{r}) + f^{\text{chain}}(\mathbf{r})]d\mathbf{r}. \tag{19}$$

At this point, the above functional does not yet contain the full information about intramolecular bonds in inhomogeneous systems captured by TPT1. As shown in Appendix A, the structure of the molecules can be captured by defining bond integrals $I_{\alpha\alpha'}(\mathbf{r})$ that are included in the Euler-Lagrange equation as

$$\rho_\alpha(\mathbf{r}) = \Lambda_i^{-3} e^{\beta\left[\mu_i - \frac{\delta F^{\text{res}}}{\delta\rho_\alpha(\mathbf{r})} - V_\alpha^{\text{ext}}(\mathbf{r})\right]} \prod_{\alpha'} I_{\alpha\alpha'}(\mathbf{r}). \tag{20}$$

The version shown here is more general than previously published expressions [38,41] because it also applies to branched molecules. In Eq. (20) the chemical potentials μ_i and thermal de Broglie wavelengths Λ_i correspond to molecules (index i) rather than segments, whereas the external potential $V_\alpha^{\text{ext}}(\mathbf{r})$ acts on individual segments. The bond integrals $I_{\alpha\alpha'}(\mathbf{r}) \neq I_{\alpha'\alpha}(\mathbf{r})$ are calculated recursively from

$$I_{\alpha\alpha'}(\mathbf{r}) = \int e^{-\beta\left[\frac{\delta F^{\text{res}}}{\delta\rho_{\alpha'}(\mathbf{r}')} + V_{\alpha'}^{\text{ext}}(\mathbf{r}')\right]} \left[\prod_{\alpha''\neq\alpha} I_{\alpha'\alpha''}(\mathbf{r}')\right] \omega_{\text{chain}}^{\alpha\alpha'}(\mathbf{r}-\mathbf{r}')d\mathbf{r}', \tag{21}$$

where the index α'' runs over all the neighbors of segment α' excluding segment α. The weight function $\omega_{\text{chain}}^{\alpha\alpha'}(\mathbf{r})$ is defined as

$$\omega_{\text{chain}}^{\alpha\alpha'}(\mathbf{r}) = \frac{1}{4\pi l_{\alpha\alpha'}^2}\delta(l_{\alpha\alpha'} - |\mathbf{r}|). \tag{22}$$

This expression is the same as in the previous publication on tangent-sphere chains [41] except for the bond-length $l_{\alpha\alpha'}$ replacing the center of mass distance of two tangentially bonded spheres $\frac{1}{2}(\sigma_\alpha + \sigma_{\alpha'})$.

C. Equation of state

With the Helmholtz energy functional in place, the equation of state of a bulk system is obtained by evaluating the functional for a system with constant densities. For convenience, we here list the relevant simplified expressions for this special case. For bulk systems, the bond integrals $I_{\alpha\alpha'}$ cancel, and the residual Helmholtz energy density f^{res} can simply be expressed as a sum of the monomer and the chain contributions

$$f^{\text{res}} = f^{\text{mono}} + f^{\text{chain}}. \tag{23}$$

The reference contribution simplifies to a modified Boublík-Mansoori-Carnahan-Starling-Leland [32,33] equation of state

$$\beta f^{\text{mono}} = \frac{6}{\pi}\left[\frac{3\zeta_1\zeta_2}{1-\zeta_3} + \frac{\zeta_2^3}{\zeta_3(1-\zeta_3)^2} + \left(\frac{\zeta_2^3}{\zeta_3^2} - \zeta_0\right)\ln(1-\zeta_3)\right], \tag{24}$$

with the modification stemming from the inclusion of the geometry coefficients A_α^* and V_α^* [Eqs. (6) and (8), respectively] in the calculation of the weighted densities

$$\zeta_0 = \frac{\pi}{6}\sum_\alpha \rho_\alpha, \qquad \zeta_1 = \frac{\pi}{6}\sum_\alpha \rho_\alpha A_\alpha^* \sigma_\alpha,$$
$$\zeta_2 = \frac{\pi}{6}\sum_\alpha \rho_\alpha A_\alpha^* \sigma_\alpha^2, \quad \zeta_3 = \frac{\pi}{6}\sum_\alpha \rho_\alpha V_\alpha^* \sigma_\alpha^3. \tag{25}$$

In a bulk system, the density ρ_α of segment α is equal to the molecular density of the component that segment α is part of. The chain contribution is calculated using Eqs. (14) and (15) together with ζ_2 and ζ_3 from Eq. (25).

1. Homosegmented fused-sphere chains

We now consider mixtures of homosegmented chains (index i) consisting of s_i segments. On each chain, the segments all have the same segment diameter σ_i and the same bond length l_i. The weighted densities in Eq. (25) simplify to

$$\zeta_0 = \frac{\pi}{6}\sum_i \rho_i s_i, \qquad \zeta_1 = \frac{\pi}{6}\sum_i \rho_i m_i \sigma_i,$$
$$\zeta_2 = \frac{\pi}{6}\sum_i \rho_i m_i \sigma_i^2, \quad \zeta_3 = \frac{\pi}{6}\sum_i \rho_i m_i^* \sigma_i^3,$$

with the molecular density ρ_i of the chains. The chain lengths m_i and m_i^* are calculated from

$$m_i = 1 + \frac{l_i}{\sigma_i}(s_i - 1) \tag{26}$$

and

$$m_i^* = 1 + \frac{1}{2}\frac{l_i}{\sigma_i}\left[3 - \left(\frac{l_i}{\sigma_i}\right)^2\right](s_i - 1), \tag{27}$$

respectively. The monomer contribution is calculated using Eq. (24) and the chain contribution simplifies to

$$\beta f^{\text{chain}} = -\sum_i \rho_i (s_i - 1)\ln y_{ii}, \tag{28}$$

with

$$y_{ii} = \frac{1}{1-\zeta_3} + \frac{3 l_i \zeta_2}{2(1-\zeta_3)^2} + \frac{(l_i\zeta_2)^2}{2(1-\zeta_3)^3}. \tag{29}$$

Although it appears an additional parameter s_i was introduced, this is not the case because the number of segments can eventually be inferred from the molecular structure (i.e., functional groups) of the real molecules that are being modeled.

2. Limiting behavior: Tangentially bonded spheres

In the limit of tangentially bonded spheres, the bond length is set to the contact value $l_{\alpha\alpha'} = \frac{1}{2}(\sigma_\alpha + \sigma_{\alpha'})$. Then, $A_\alpha^* = V_\alpha^* = 1$ and $b_{\alpha\alpha'} = \frac{2\sigma_\alpha\sigma_{\alpha'}}{\sigma_\alpha + \sigma_{\alpha'}}$. Therefore, the functional and equation of state for the fused chain model simplify to Wertheim's theory with a hard-sphere reference fluid.

3. Limiting behavior: Totally fused spheres

For dimers ($\sigma_1 > \sigma_2$), the limit of total fusion is reached for $l_{12} = \frac{1}{2}(\sigma_1 - \sigma_2)$. Then, the equation of state simplifies to that of a hard-sphere fluid. In this case $\delta_{12} = \frac{\sigma_1}{2}$ and $\delta_{21} = -\frac{\sigma_2}{2}$ and from Eqs. (6) and (8), $A_1^* = V_1^* = 1$ and $A_2^* = V_2^* = 0$. Therefore, the weighted densities ζ_1, ζ_2 and ζ_3 simplify to those of a pure system of hard spheres of diameter σ_1. This is not the case for ζ_0 which remains at double the value of a hard-sphere system. Using these weighted densities in Eq. (24) thus leads to

$$\beta f^{\text{mono}} = \beta f^{\text{hs}} - \rho\ln(1-\zeta_3). \tag{30}$$

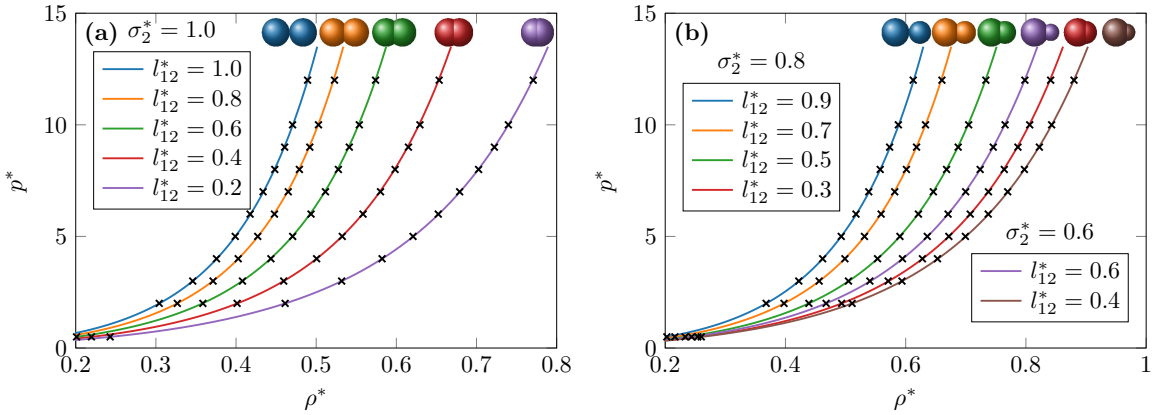

FIG. 3. Reduced pressure p^* of (a) symmetric and (b) asymmetric dimers ($\sigma_1^* = 1.0$) as function of the reduced density ρ^*. Comparison of equation of state results (lines) and NpT-MC simulations (crosses).

However, since $b_{12} = 0$ in the limit of total fusion, the chain contribution simplifies to $\beta f^{\text{chain}} = \rho \ln(1 - \zeta_3)$ exactly what is needed to give the desired result $f^{\text{res}} = f^{\text{mono}} + f^{\text{chain}} = f^{\text{hs}}$, for this case.

For chains with more than two segments, this line of argumentation is only valid, if terminal segments can subsequently be fused fully into their only neighbor. This is not the case if one segment has two neighbors that both have a larger diameters than itself. For homosegmented chains, however, the limit of total fusion is correct: for $l_i = 0$, we find $m_i = m_i^* = 1$ and therefore ζ_1, ζ_2 and ζ_3 simplify to those of a hard-sphere system. That part of the monomer contribution stemming from the difference between ζ_0 of the reference fluid and the hard-sphere system again cancels with the chain contribution that simplifies to

$$\beta f^{\text{chain}} = \sum_i \rho_i (s_i - 1) \ln(1 - \zeta_3). \tag{31}$$

III. RESULTS AND DISCUSSION

In the following paragraphs, we compare the predictions of the fused chain functional developed in Sec. II to molecular simulation results. Bulk pressures were calculated using isobaric-isothermal NpT Monte Carlo (MC) simulations, while the density profiles in slit pores were obtained from grand-canonical μVT MC simulations. Details of the molecular simulations are given in Sec. B1 and the full simulation results are available as Supplemental Material [43]. The source code (Rust with Python bindings) for the fused chain Helmholtz energy functional used to calculate both homogeneous and inhomogeneous systems is published as part of the FeO_s project [44].

All results are given in reduced units $\rho^* = \rho x^3$, $p^* = \frac{p x^3}{k_B T}$, $\mu^* = \frac{\mu}{k_B T}$, and $z^* = \frac{z}{x}$, where x is an arbitrary reference length (for all practical purposes $x = 1$ Å). Since we consider hard particles, the temperature T has no effect on reduced properties. The reduced thermal de Broglie wavelength Λ^* that contributes to the ideal gas chemical potential is set to unity as its value has no effect on the pressure or the density profiles.

A. Bulk pressure

To validate the bulk limit of the fused chain functional developed in Sec. II, reduced pressures are compared to results obtained from NpT-MC simulations. In Fig. 3 we show the results for symmetric and asymmetric dimers with varying degree of fusion. For the full range of bond lengths the model predictions are in excellent quantitative agreement to simulation data, even for highly asymmetrical dimers.

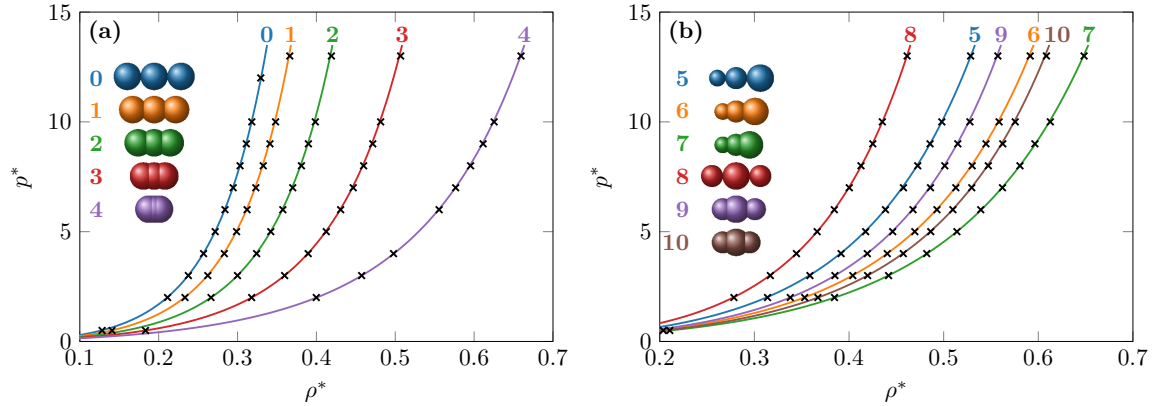

FIG. 4. Reduced pressure p^* of (a) homosegmented and (b) heterosegmented trimers as function of the reduced density ρ^*. Comparison of equation of state results (lines) and NpT-MC simulations (crosses). The parameters of the trimers are given in Table I.

TABLE I. Segment diameters and bond lenghts of the trimers studied in Fig. 4. We also include the minimum bond angle used in the Monte Carlo simulations to avoid overlapping between the outer segments.

Trimer #	σ_1^*	σ_2^*	σ_3^*	l_{12}^*	l_{23}^*	$\theta_{\min}$
0	1.0	1.0	1.0	1.0	1.0	60.000°
1				0.8	0.8	77.364°
2				0.6	0.6	106.26°
3				0.4	0.4	132.84°
4				0.2	0.2	156.93°
5	0.6	0.8	1.0	0.7	0.9	58.412°
6				0.5	0.7	81.787°
7				0.5	0.5	103.29°
8	0.8	1.0	0.8	0.9	0.9	52.776°
9				0.5	0.7	81.204°
10				0.5	0.5	94.313°

Trimers are investigated in Fig. 4. For homosegmented trimers with bond lengths as short as $l^* = 0.2$ and also heterosegmented trimers with various shapes, agreement between the equation of state and Monte Carlo simulations is again excellent. The model parameters for the trimers are shown in Table I. The minimum bond angle $\theta_{\min}$ is an important property of the underlying molecular model and is thus required as an input to the MC simulations to capture the molecular model accurately. It is not, however, a parameter in the equation of state, because TPT1 only describes correlations between nearest-neighbor segments within a chain. To explicitly include the effect of the (minimum) bond angle, at least a second order thermodynamic perturbation theory (TPT2) is required. Details about the calculation of $\theta_{\min}$ can be found in Sec. B1.

For longer molecules, we consider homosegmented chains with 5, 10, and 20 segments (Fig. 5). For practical reasons (see Sec. B1), we only consider chains with reduced bond lengths $l^* > 0.5$. While the agreement between simulations and theory is again satisfying, we observe a shortcoming of the underlying TPT1, which was shown to be unable to accurately describe the low-density behavior of long chain molecules [5,45]. To emphasize this, we show the absolute value of percentage deviations of the predicted pressures with respect to MC simulation results in the lower part of Fig. 5. The error is highest for low densities and long chains. As a reference, the errors for trimers and dimers are below 2.5% and 1.2%, respectively. An important observation for this study is, that going from tangent-sphere chains to fused-sphere chains does not increase the error further. The reason for the lower accuracy of TPT1 (and its higher-order variants, TPT2, TPT3, and so on) can be attributed to the single-chain approximation. The underlying assumption is that the change in free energy due to chain formation can be described by that of a single chain in a system of monomers [46]. While for high densities, the local environment of a chain in a fluid of chains is indeed very similar to that of a chain in a fluid of monomers, that is not the case at low densities. This is reflected by the pair-excluded volume of two chains and that of a chain and monomers, which is significantly different.

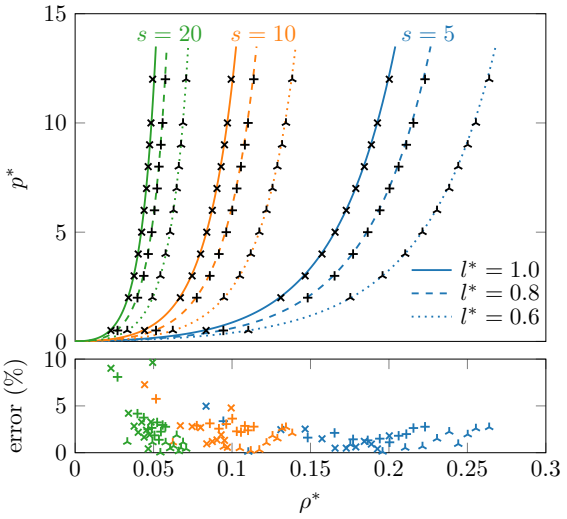

FIG. 5. Reduced pressure p^* and relative error of homosegmented chains ($\sigma^* = 1.0$) with different numbers of segments s and bond lengths l^* as function of the reduced density ρ^*. Comparison of equation of state results (lines) and NpT-MC simulations (symbols).

Therefore, to improve the description of the low-density behavior, one must go beyond the single-chain approximation that underlies TPT1 [46], or devise some (empirical) procedure that corrects the low-density limit of the chain functional [47,48].

The capability of the fused-sphere chain equation of state is further analyzed in a study of two sets of binary mixtures. In Fig. 6 mixtures of fused dimers with varying bond lengths and a trimer with a large central segment is studied. In Fig. 7, a mixture of fused homosegmented chains with different lengths and a larger fused dimer is studied. In all cases, the agreement between the equation of state predictions and results from molecular simulations is excellent, showing

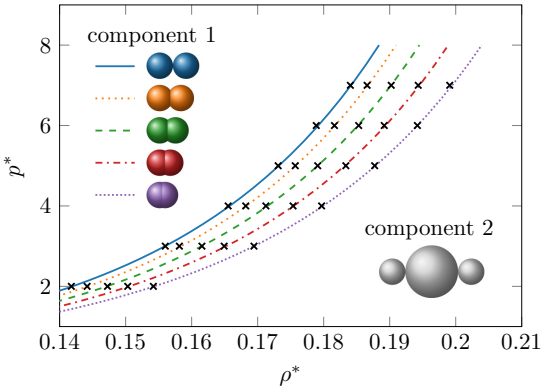

FIG. 6. Reduced pressure p^* of several equimolar binary mixtures as function of the reduced (total) density ρ^*. Comparison of equation of state results (lines) and NpT-MC simulations (crosses). Component 1 consists of homosegmented dimers with diameter $\sigma^* = 1$ and varying bond lengths $l^* \in \{0.2, 0.4, 0.6, 0.8, 1.0\}$. Component 2 is a heterosegmented trimer with $\sigma_1^* = \sigma_3^* = 1$, $\sigma_2^* = 2$, and $l_{12}^* = l_{23}^* = 1.5$.

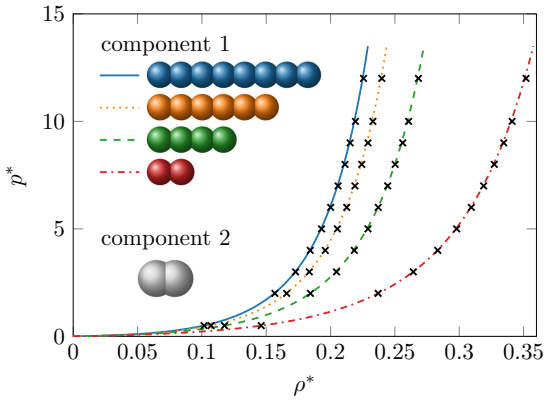

FIG. 7. Reduced pressure p^* of several binary mixtures as function of the reduced (total) density ρ^*. Comparison of equation of state results (lines) and NpT-MC simulations (crosses). Component 1 consists of $N_1 \in \{300, 150, 100, 75\}$ homosegmented chains with $s \in \{2, 4, 6, 8\}$ segments, $\sigma^* = 1$ and $l^* = 0.8$. Component 2 consists of $N_2 = 300$ homosegmented dimers with $\sigma^* = 1.4$ and $l^* = 0.7$.

that the remarkable accuracy of the BMCSL equation of state with TPT1 for mixtures of tangent-sphere chains is preserved in our model.

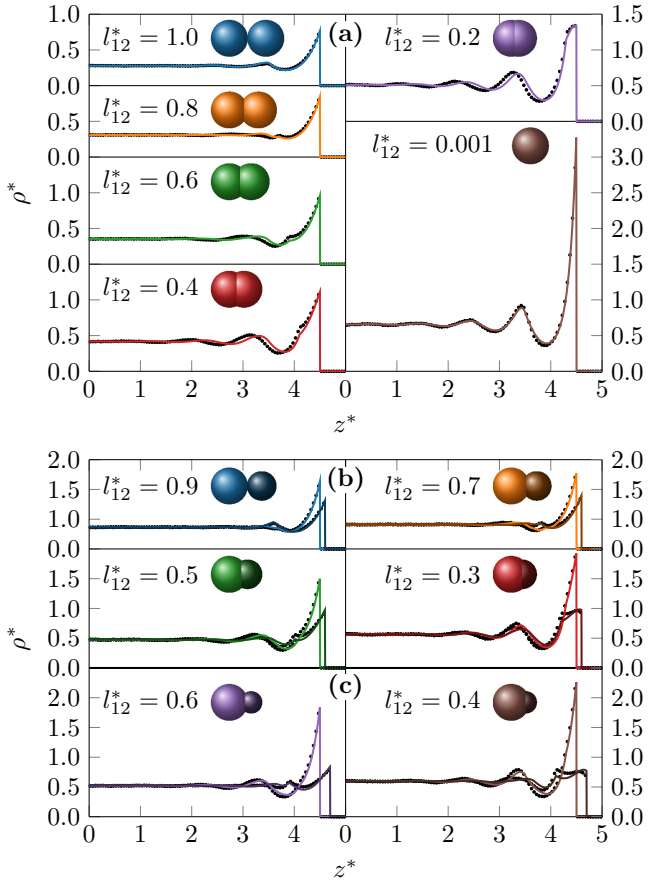

FIG. 8. Density profiles of dimers ($\sigma_1^* = 1$, $\mu^* = 6$) with (a) $\sigma_2^* = 1$, (b) $\sigma_2^* = 0.8$, and (c) $\sigma_2^* = 0.6$ in a slit pore. Comparison of density functional theory results (lines) with μVT-MC simulations (dots).

B. Density in a slit pore

To assess the predictive capability of the Helmholtz energy functional, the density profiles of fused chain molecules in slit pores are compared to the results of grand canonical Monte Carlo simulations. The external potential used to model the interaction between the molecules and the hard wall is given by

$$V_\alpha^{\text{ext}}(z) = \begin{cases} \infty & |z| \geqslant \frac{w-\sigma_\alpha}{2}, \\ 0 & |z| < \frac{w-\sigma_\alpha}{2}. \end{cases} \tag{32}$$

The reduced pore width is set to $w^* = 10$.

In Fig. 8, the results for symmetric and asymmetric dimers are shown. The density functional theory model reproduces all qualitative features of the molecular simulation results: the accumulation of molecules in adsorbed layers, the effect of the size of the segments on the locations of the first layer, and the reduction of the contact density for the smaller segments. As a caveat, the width of the adsorbed layers is slightly underpredicted by the DFT results. This is not the case for the almost entirely fused dimer ($l_{12}^* = 0.001$), which proves that this caveat is not due to incorrect limiting behavior but rather a slight inaccuracy that occurs for strongly fused dimers.

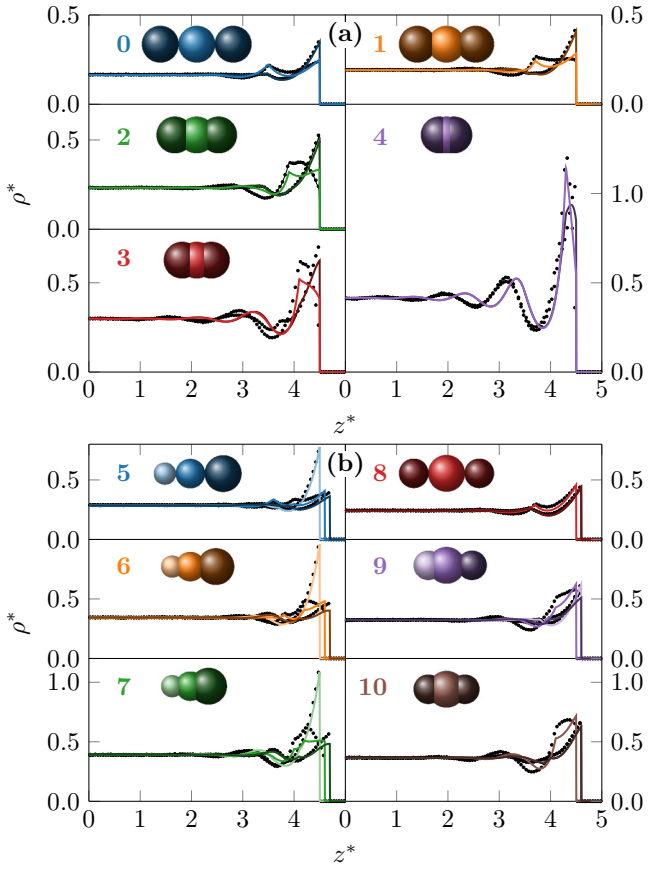

FIG. 9. Density profiles of (a) homosegmented and (b) heterosegmented trimers ($\mu^* = 6$) in a slit pore. Comparison of density functional theory results (lines) with μVT-MC simulations (dots). The parameters of the trimers are given in Table I. For trimer 2, the μVT simulation results are additionally validated with independent NVT simulations (black lines).

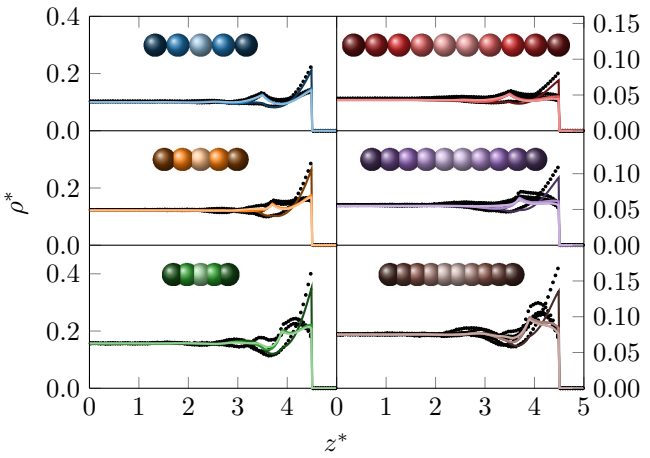

FIG. 10. Density profiles of homosegmented pentamers ($s = 5$, $\sigma^* = 1$, $\mu^* = 10$) and decamers ($s = 10$, $\sigma^* = 1$, $\mu^* = 14$) with bond lengths $l^* = 1.0$, $l^* = 0.8$, and $l^* = 0.6$. Comparison of density functional theory results (lines) with μVT-MC simulations (dots).

The problem persists for the trimers we considered in Fig. 9. In particular for the strongly fused trimers, the thickness of the adsorbed layers is underestimated by the DFT model. Further, we must concede, that the description of the density of the central segment for the homosegmented trimers deviates from the simulation results. This effect becomes more pronounced for small bond lengths. To ensure the consistency of the DFT implementation and the simulations, we verified that the contact densities ρ_α^c of both the DFT model and the simulations are in accordance with the sum rule [30]

$$\beta p = \sum_\alpha \rho_\alpha^c. \tag{33}$$

However, this exact relation unfortunately does not provide any checks on the contact density of individual segments. Due to the increasing minimal bond angle and the corresponding increased stiffness, the strongly fused trimers 3 and 4 resemble hard spherocylinders. In the Helmholtz energy functional for hard spherocylinders by Hansen-Goos and Mecke [35], the nonsphericity of the particles is accounted for by using an additional rotational degree of freedom. As their model shows an excellent agreement with simulation data for particles at hard walls, it could be used to point towards improvements of the present model in the limit of short bond lengths.

For homosegmented chains, Fig. 10 shows the density profiles of pentamers ($s = 5$, $\mu^* = 10$) and decamers ($s = 10$, $\mu^* = 14$). As the calculations are done at low densities, the agreement between DFT and simulations is impaired by the deviation that TPT1 shows in the low density limit. Both, the DFT and the molecular simulations predict that the density profiles of inner segments become less distinguishable for longer chains. However, this effect is somewhat overestimated by the DFT model.

IV. CONCLUSION

In this work, we derived a Helmholtz energy functional for fused hard chains by applying Wertheim's TPT1 to a system of hard-sphere fragments. The model describes the molecules using the same parameters as would be required in molecular simulations of fused chains; namely, the segment diameters and bond-lengths. No adjustable parameters are involved. The functional qualitatively captures the orientation and structure of hard fused chains in a slit pore and leads to excellent predictions for the bulk equation of state. For longer chains, the accuracy in the overall description of inhomogeneous phases decreases somewhat. Part of these inaccuracies are caused by TPT1, which is known to be inaccurate for low densities.

The equation of state presented in this work is sufficiently simple to be applied as a reference for a perturbation theory, such as statistical associating fluid theory (SAFT). Extending SAFT approaches to a well-defined molecular model of fused-sphere chains with bond lengths as a physical meaningful parameter is of great benefit because the model is then in better alignment with force fields used in molecular simulations. In particular, this extension offers great perspectives for developing group-contribution models. Further, for inhomogeneous systems, the proposed model allows a local resolution of actual chemical groups. When comparing DFT results to molecular simulations of real fluids, the comparison is typically impaired by the different molecular descriptions used in the DFT and molecular simulations approaches. Force fields that are used to parametrize real fluids, such as TraPPE [49] or TAMie [50], describe molecules using bond lengths much shorter than the tangential contact distance for any physically meaningful definition of the segment radii. A heterosegmented Helmholtz energy based on the fused chain model presented here enables a more direct comparison between DFT and simulation results of density profiles of individual segments/interaction-sites in interfaces or porous media.

Finally, we emphasize the benefit of starting the development of the equation of state from the more general inhomogeneous and heterosegmented system and proceed towards a simplified case. With this approach, we obtain a highly accurate bulk equation of state for homosegmented chains as a corollary of the more general Helmholtz energy functional.

ACKNOWLEDGMENTS

The authors thank the German Research Foundation (DFG) for financial support within the Cluster of Excellence in Simulation Technology (Grant No. EXC 2075, Project ID No. 390740016) at the University of Stuttgart. The authors acknowledge support by the state of Baden-Württemberg through bwHPC. The authors thank Prof. Thijs Vlugt for generously providing us with his Recoil-growth MC code and for his assistance in extending the code to our purposes.

APPENDIX A: DERIVATION OF THE EULER-LAGRANGE EQUATION FOR BRANCHED FUSED CHAINS

The derivation of Eqs. (20) and (21) follows the method outlined by Jain *et al.* [38] and refined by Rehner *et al.* [41]. The derivation is the same for fused-sphere chains and tangent-sphere chains. The reason why it is presented here, is that Eqs. (20) and (21) generalize the concept to branched

molecules in a more concise and general way as compared to the expressions published previously [51].

The starting point is the inhomogeneous version of Wertheim's TPT1 [39], that describes the Helmholtz energy of systems of associating spheres as

$$\beta F^{\text{bond}} = \int \sum_{\alpha} \sum_{\alpha'} \rho_{\alpha}(\mathbf{r}) \left(\ln \chi_{\alpha\alpha'}(\mathbf{r}) - \frac{\chi_{\alpha\alpha'}(\mathbf{r})}{2} + \frac{1}{2} \right) d\mathbf{r}. \tag{A1}$$

The index α runs over all segments in the system and the sum over α' is over all segments bonded to α. The values of the fractions of nonbonded segments $\chi_{\alpha\alpha'}$ is determined implicitly by

$$\chi_{\alpha\alpha'}(\mathbf{r}) = \left[1 + \int \rho_{\alpha'}(\mathbf{r}') \chi_{\alpha'\alpha}(\mathbf{r}') \Delta_{\alpha\alpha'}(\mathbf{r}, \mathbf{r}') d\mathbf{r}' \right]^{-1}. \tag{A2}$$

The association strength $\Delta_{\alpha\alpha'}(\mathbf{r}, \mathbf{r}')$ can be approximated by

$$\Delta_{\alpha\alpha'}(\mathbf{r}, \mathbf{r}') = K \omega^{\alpha\alpha'}_{\text{chain}}(\mathbf{r} - \mathbf{r}') \sqrt{y_{\alpha\alpha'}(\mathbf{r}) y_{\alpha\alpha'}(\mathbf{r}')} \tag{A3}$$

with the weight function $\omega^{\alpha\alpha'}_{\text{chain}}(\mathbf{r})$ as given in Eq. (22). The constant K contains the energy parameter of the association potential and goes to infinity for complete association. The model for the cavity correlation function at contact $y_{\alpha\alpha'}$ can differ for different applications. To be able to combine all fluid-specific models in one residual Helmholtz energy functional, the cavity correlation is contained in a chain contribution,

$$\beta F^{\text{chain}} = -\frac{1}{2} \int \sum_{\alpha} \sum_{\alpha'} \rho_{\alpha}(\mathbf{r}) \ln y_{\alpha\alpha'}(\mathbf{r}) d\mathbf{r}, \tag{A4}$$

and the properties $\hat{\chi}_{\alpha\alpha'} = \chi_{\alpha\alpha'} \sqrt{y_{\alpha\alpha'}}$ and

$$\beta \hat{F}^{\text{bond}} = \beta F^{\text{bond}} - \beta F^{\text{chain}} \tag{A5}$$

$$= \int \sum_{\alpha} \sum_{\alpha'} \rho_{\alpha}(\mathbf{r}) \left[\ln \hat{\chi}_{\alpha\alpha'}(\mathbf{r}) - \frac{\hat{\chi}_{\alpha\alpha'}(\mathbf{r})}{2\sqrt{y_{\alpha\alpha'(\mathbf{r})}}} + \frac{1}{2} \right] d\mathbf{r} \tag{A6}$$

are defined. In the limit of complete association ($\hat{\chi}_{\alpha\alpha'} \to 0$), the functional derivative of this modified bond contribution simplifies to [41]

$$\frac{\delta \beta \hat{F}^{\text{bond}}}{\delta \rho_{\alpha}(\mathbf{r})} = \sum_{\alpha'} \ln \hat{\chi}_{\alpha\alpha'}. \tag{A7}$$

The total Helmholtz energy now consists of an ideal gas contribution, the modified bond contribution, the chain contribution and the contribution from the monomers:

$$F = F^{\text{ig}} + \hat{F}^{\text{bond}} + \underbrace{F^{\text{chain}} + F^{\text{mono}}}_{F^{\text{res}}}. \tag{A8}$$

If additional contributions are present due to attractive interactions, they can be included in the residual Helmholtz energy F^{res} without additional modifications to the framework. Equations (A7) and (A8) can now be used in the general Euler-Lagrange equation

$$\frac{\delta F}{\delta \rho_{\alpha}(\mathbf{r})} = \mu_{\alpha} - V^{\text{ext}}_{\alpha}(\mathbf{r}), \tag{A9}$$

to give

$$\ln \left(\rho_{\alpha}(\mathbf{r}) \Lambda^3_{\alpha} \right) + \sum_{\alpha'} \ln \hat{\chi}_{\alpha\alpha'}(\mathbf{r}) + \frac{\delta \beta F^{\text{res}}}{\delta \rho_{\alpha}(\mathbf{r})} = \beta \left[\mu_{\alpha} - V^{\text{ext}}_{\alpha}(\mathbf{r}) \right]. \tag{A10}$$

Equation (A10) has to be solved simultaneously with the equation for $\hat{\chi}_{\alpha\alpha'}$,

$$\hat{\chi}_{\alpha\alpha'}(\mathbf{r})^{-1} = K \int \rho_{\alpha'}(\mathbf{r}') \hat{\chi}_{\alpha'\alpha}(\mathbf{r}') \omega^{\alpha\alpha'}_{\text{chain}}(\mathbf{r} - \mathbf{r}') d\mathbf{r}', \tag{A11}$$

which follows from Eqs. (A2) and (A3) in the limit of complete association ($K \to \infty$). Equation (A10) for segment α' can be rewritten as

$$\rho_{\alpha'}(\mathbf{r}) \hat{\chi}_{\alpha'\alpha}(\mathbf{r}) = \Lambda^{-3}_{\alpha'} e^{\beta \left(\mu_{\alpha'} - \frac{\delta F^{\text{res}}}{\delta \rho_{\alpha'}(\mathbf{r})} - V^{\text{ext}}_{\alpha'}(\mathbf{r}) \right)} \prod_{\alpha'' \neq \alpha} \hat{\chi}_{\alpha'\alpha''}(\mathbf{r})^{-1}, \tag{A12}$$

where α is one of the neighbors of α' and the product over α'' runs over all *other* neighbors of α'. Equation (A12) can be used in Eq. (A11) resulting in

$$\hat{\chi}_{\alpha\alpha'}(\mathbf{r})^{-1} = K \Lambda^{-3}_{\alpha'} e^{\beta \mu_{\alpha'}} \int e^{-\beta \left[\frac{\delta F^{\text{res}}}{\delta \rho_{\alpha'}(\mathbf{r}')} + V^{\text{ext}}_{\alpha'}(\mathbf{r}') \right]} \times \left[\prod_{\alpha'' \neq \alpha} \hat{\chi}_{\alpha'\alpha''}(\mathbf{r}')^{-1} \right] \omega^{\alpha\alpha'}_{\text{chain}}(\mathbf{r} - \mathbf{r}') d\mathbf{r}'. \tag{A13}$$

As long as there are no cycles in the molecule, this expression recursively defines the values of $\hat{\chi}_{\alpha\alpha'}$ with the recursion ending at the terminal segments for which the product over α'' vanishes. If Eq. (A13) is used in the Euler-Lagrange Eq. (A10), then it can be observed that the expression $\Lambda^{-3}_{\alpha} e^{\beta \mu_{\alpha}}$ appears exactly once for every segment of the molecule. Therefore, it can be separated out from the values of $\hat{\chi}_{\alpha\alpha'}$ leaving behind the bond integrals $I_{\alpha\alpha'}$. In the Euler-Lagrange equation, the chemical potential of the molecule $\mu_i = \sum_{\alpha \in i} \mu_{\alpha}$ can be identified. In a similar expression for the thermal de Broglie wavelength,

$$\Lambda^3_i = K \prod_{\alpha \in i} \frac{\Lambda^3_{\alpha}}{K}, \tag{A14}$$

the reduction of the degrees of freedom of the molecule compared to the degrees of freedom of free segments is reflected. The simplified expressions for the Euler-Lagrange equation,

$$\rho_{\alpha}(\mathbf{r}) = \Lambda^{-3}_i e^{\beta \left(\mu_i - \frac{\delta F^{\text{res}}}{\delta \rho_{\alpha}(\mathbf{r})} - V^{\text{ext}}_{\alpha}(\mathbf{r}) \right)} \prod_{\alpha'} I_{\alpha\alpha'}(\mathbf{r}), \tag{A15}$$

and the bond integrals

$$I_{\alpha\alpha'}(\mathbf{r}) = \int e^{-\beta \left[\frac{\delta F^{\text{res}}}{\delta \rho_{\alpha'}(\mathbf{r}')} + V^{\text{ext}}_{\alpha'}(\mathbf{r}') \right]} \left[\prod_{\alpha'' \neq \alpha} I_{\alpha'\alpha''}(\mathbf{r}') \right] \omega^{\alpha\alpha'}_{\text{chain}}(\mathbf{r} - \mathbf{r}') d\mathbf{r}' \tag{A16}$$

follow. The notation that relies heavily on sums over all segments bonded to a specific segment can appear clumsy to implement. However, by choosing an appropriate data structure like a directed graph with the bond integrals as edge weights, the equations can be transformed to code straightforwardly.

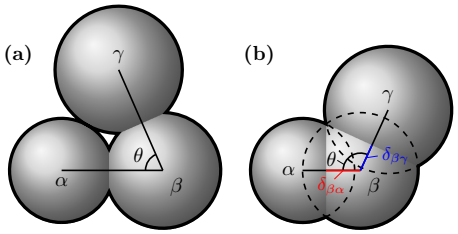

FIG. 11. Minimum bond angle θ for (a) slightly fused trimers and (b) strongly fused trimers.

APPENDIX B: MOLECULAR SIMULATION DETAILS

1. Angle potential for fused hard-sphere chain molecules

Due to the fusing of the spheres, angle constraints have to be implemented to generate valid configurations in a molecular simulation. For slightly fused trimers like the one shown in Fig. 11(a), an overlap between segments α and γ can be avoided by simply applying the normal hard-sphere interaction potential. For strongly fused trimers as shown in Fig. 11(b), an overlap between the outer segments is allowed as long as the overlap is within the central segment. Therefore, a hard-sphere pair potential can not be used between the outer segments. We define a hard bond-angle potential that is 0 for bond angles above the minimum angle $\theta_{\min}$ and infinite below. For slightly fused trimers, the value for $\theta_{\min}$ follows from the law of cosines as

$$\cos\theta_{\min} = \frac{4\left(l_{\alpha\beta}^2 + l_{\beta\gamma}^2\right) - (\sigma_\alpha + \sigma_\gamma)^2}{8 l_{\alpha\beta} l_{\beta\gamma}}$$

$$\text{if} \quad 4\frac{\sigma_\alpha l_{\beta\gamma}^2 + \sigma_\gamma l_{\alpha\beta}^2}{\sigma_\alpha + \sigma_\gamma} - \sigma_\alpha\sigma_\gamma \geqslant \sigma_\beta^2 \;\Leftrightarrow\; \text{slightly fused.}$$

The distinction between a slightly and a strongly fused trimer is that the distance between the point of contact between the outer spheres to the center of the middle sphere is larger than the radius of the middle sphere. For strongly fused trimers, the minimum bond angle is

$$\cos\theta_{\min} = \frac{4\delta_{\beta\alpha}\delta_{\beta\gamma} - \sqrt{\left(\sigma_\beta^2 - 4\delta_{\beta\alpha}^2\right)\left(\sigma_\beta^2 - 4\delta_{\beta\gamma}^2\right)}}{\sigma_\beta^2}$$

$$\text{if} \quad 4\frac{\sigma_\alpha l_{\beta\gamma}^2 + \sigma_\gamma l_{\alpha\beta}^2}{\sigma_\alpha + \sigma_\gamma} - \sigma_\alpha\sigma_\gamma < \sigma_\beta^2 \;\Leftrightarrow\; \text{strongly fused.}$$

For longer chains these expressions can be used for every triplet individually, however, extra care has to be applied when the fusion is strong enough that there can also be a permissable overlap between further apart segments. For homosegmented trimers, the minimum bond angle simplifies to

$$\cos\theta_{\min} = \begin{cases} \frac{2l^2-\sigma^2}{2l^2} & l \geqslant \frac{\sigma}{\sqrt{2}}, \\ \frac{2l^2-\sigma^2}{\sigma^2} & l < \frac{\sigma}{\sqrt{2}}. \end{cases} \tag{B1}$$

The critical bond length, i.e., the bond length below which an n-segment angle potential has to be implemented instead of using hard-sphere pair potentials can be found as

$$l = \sigma \sin\left(\frac{\pi}{2n-2}\right). \tag{B2}$$

Therefore, the shortest bond length for which angle potentials for three consecutive segments and hard-sphere interactions for all other interactions can be employed is $l = \sigma \sin(\frac{\pi}{6}) = \frac{\sigma}{2}$.

2. *NpT*-MC simulations

The bulk density of hard-sphere chain fluids was calculated for specified bulk pressures p^*, based on isobaric-isothermal NpT-MC simulations [52] using an in-house MC code. The code was validated to the molecular dynamics simulation results for the pressure of tangent hard-sphere chains by Zmpitas [45] and to μVT-MC simulation results for the pressure of fused dimers and trimers generated according to the procedure outlined in the next section. The NpT-code and the μVT-code were developed independently and can thus be used for cross validation.

For generating the bulk density, we used a cubic box containing between $N_s = 1500$ and $N_s = 2000$ segments. Periodic boundary conditions were applied. We employed at least 10^6 MC cycles for equilibration, and 10^6 cycles for production, with each cycle comprising N MC moves. The MC moves considered were translation [52], rotation [52], configurational bias regrowth [53,54], crank-shaft moves [55,56], and volume moves [52], with relative probabilities 0.4, 0.4, 0.18, 0, 0.02 (trimers); 0.286, 0.286, 0.129, 0.286, 0.0143 (5-mers and 10-mers), and 0.22, 0.22, 0.1, 0.44, 0.011 (20-mers), respectively. During equilibration, the step-size for translation, rotation and volume moves was adjusted to obtain approximately 20% acceptance. For the configurational bias regrowth move, we chose a random segment as the starting segment and regrew the molecule in a random direction (forward or backward) using six trial directions for each new segment. The crank-shaft moves were combined with a configurational bias scheme, using six trial angles for the rotated segment. The standard error of the sampled density was estimated by dividing the production part of the simulation into five blocks and calculating the standard deviation of the block averages with respect to the average over all five blocks.

3. *μVT*-MC simulations

Hard-sphere chain fluids between two parallel hard walls were simulated based on grand-canonical μVT Monte Carlo simulations. [52] The plates were placed parallel to the z direction at a reduced distance $w^* = 10$, while periodic boundary conditions were applied in the other directions. The box was cubic, with a volume $V = w^3$. The types of moves considered were translation, rotation, insertion, deletion, and regrowth with relative probabilities 0.25, 0.25, 0.25, 0.25, 0 for dimers, 0.2, 0.2, 0.2, 0.2, 0.2 for trimers and 5-mers, and 0.15, 0.15, 0.2, 0.2, 0.3 for 10-mers. We applied a configurational-bias scheme with 10 trial directions [53,54] to improve the sampling of chain configurations. Equilibration was performed for 10^7 trial moves and production was conducted for 4×10^7 trial moves.

The full simulation results are available as Supplemental Material [43].

[1] M. S. Wertheim, J. Stat. Phys. **35**, 19 (1984).
[2] M. S. Wertheim, J. Stat. Phys. **35**, 35 (1984).
[3] M. S. Wertheim, J. Stat. Phys. **42**, 459 (1986).
[4] M. S. Wertheim, J. Stat. Phys. **42**, 477 (1986).
[5] W. Zmpitas and J. Gross, Fluid Phase Equilib. **428**, 121 (2016).
[6] W. G. Chapman, K. E. Gubbins, G. Jackson, and M. Radosz, Ind. Eng. Chem. Res. **29**, 1709 (1990).
[7] A. Gil-Villegas, A. Galindo, P. J. Whitehead, S. J. Mills, G. Jackson, and A. N. Burgess, J. Chem. Phys. **106**, 4168 (1997).
[8] F. J. Blas and L. F. Vega, Ind. Eng. Chem. Res. **37**, 660 (1998).
[9] T. Lafitte, A. Apostolakou, C. Avendaño, A. Galindo, C. S. Adjiman, E. A. Müller, and G. Jackson, J. Chem. Phys. **139**, 154504 (2013).
[10] J. Gross and G. Sadowski, Ind. Eng. Chem. Res. **40**, 1244 (2001).
[11] J. Gross, O. Spuhl, F. Tumakaka, and G. Sadowski, Ind. Eng. Chem. Res. **42**, 1266 (2003).
[12] E. Sauer, M. Stavrou, and J. Gross, Ind. Eng. Chem. Res. **53**, 14854 (2014).
[13] V. Papaioannou, T. Lafitte, C. Avendaño, C. S. Adjiman, G. Jackson, E. A. Müller, and A. Galindo, J. Chem. Phys. **140**, 054107 (2014).
[14] W. A. Steele and S. I. Sandler, J. Chem. Phys. **61**, 1315 (1974).
[15] F. Kohler, W. Marius, N. Quirke, J. Perram, C. Hoheisel, and H. Breitenfelder-Manske, Mol. Phys. **38**, 2057 (1979).
[16] T. W. Melnyk and W. R. Smith, Mol. Phys. **40**, 317 (1980).
[17] D. Tildesley and W. Streett, Mol. Phys. **41**, 85 (1980).
[18] T. Boublík, J. Chem. Phys. **63**, 4084 (1975).
[19] T. Boublík and I. Nezbeda, Chem. Phys. Lett. **46**, 315 (1977).
[20] T. Boublík, Mol. Phys. **68**, 191 (1989).
[21] T. Boublík, C. Vega, and M. Diaz–Peña, J. Chem. Phys. **93**, 730 (1990).
[22] J. M. Walsh and K. E. Gubbins, J. Phys. Chem. **94**, 5115 (1990).
[23] M. D. Amos and G. Jackson, J. Chem. Phys. **96**, 4604 (1992).
[24] S. Phan, E. Kierlik, and M. L. Rosinberg, J. Chem. Phys. **101**, 7997 (1994).
[25] Y. Zhou, C. K. Hall, and G. Stell, J. Chem. Phys. **103**, 2688 (1995).
[26] A. Dominik, P. Jain, and W. G. Chapman, Mol. Phys. **103**, 1387 (2005).
[27] R. Evans, Adv. Phys. **28**, 143 (1979).
[28] Y. Rosenfeld, Phys. Rev. Lett. **63**, 980 (1989).
[29] M. S. Wertheim, Phys. Rev. Lett. **10**, 321 (1963).
[30] R. Roth, R. Evans, A. Lang, and G. Kahl, J. Phys.: Condens. Matter **14**, 12063 (2002).
[31] Y.-X. Yu and J. Wu, J. Chem. Phys. **117**, 10156 (2002).
[32] T. Boublík, J. Chem. Phys. **53**, 471 (1970).
[33] G. A. Mansoori, N. F. Carnahan, K. E. Starling, and T. W. Leland, J. Chem. Phys. **54**, 1523 (1971).
[34] Y. Rosenfeld, Phys. Rev. E **50**, R3318 (1994).
[35] H. Hansen-Goos and K. Mecke, Phys. Rev. Lett. **102**, 018302 (2009).
[36] H. Hansen-Goos and K. Mecke, J. Phys.: Condens. Matter **22**, 364107 (2010).
[37] M. Marechal, H. H. Goetzke, A. Härtel, and H. Löwen, J. Chem. Phys. **135**, 234510 (2011).
[38] S. Jain, A. Dominik, and W. G. Chapman, J. Chem. Phys. **127**, 244904 (2007).
[39] C. J. Segura, W. G. Chapman, and K. P. Shukla, Mol. Phys. **90**, 759 (1997).
[40] R. Roth, J. Phys.: Condens. Matter **22**, 063102 (2010).
[41] P. Rehner, B. Bursik, and J. Gross, Ind. Eng. Chem. Res. **60**, 7111 (2021).
[42] S. Tripathi and W. G. Chapman, J. Chem. Phys. **122**, 094506 (2005).
[43] See Supplemental Material at http://link.aps.org/supplemental/10.1103/PhysRevE.105.034110 for the full simulation results.
[44] Published on https://github.com/feos-org/feos-fused-chains.
[45] W. Zmpitas and J. Gross, Fluid Phase Equilib. **416**, 18 (2016).
[46] W. Zmpitas and J. Gross, J. Chem. Phys. **150**, 244902 (2019).
[47] T. van Westen, B. Oyarzún, T. J. Vlugt, and J. Gross, Mol. Phys. **112**, 919 (2014).
[48] J. R. Elliott, J. Phys. Chem. B **125**, 4494 (2021).
[49] M. G. Martin and J. I. Siepmann, J. Phys. Chem. B **102**, 2569 (1998).
[50] A. Hemmen and J. Gross, J. Phys. Chem. B **119**, 11695 (2015).
[51] Y. Zhang, A. Valiya Parambathu, and W. G. Chapman, J. Chem. Phys. **149**, 064904 (2018).
[52] D. Frenkel and B. Smit, *Understanding Molecular Simulation: From Algorithms to Applications*, 2nd ed. (Academic Press, San Diego, CA, 2002).
[53] D. Frenkel, G. C. A. M. Mooij, and B. Smit, J. Phys.: Condens. Matter **3**, 3053 (1991).
[54] J. I. Siepmann and D. Frenkel, Mol. Phys. **75**, 59 (1992).
[55] X. Li and Y. C. Chiew, J. Chem. Phys. **101**, 2522 (1994).
[56] F. A. Escobedo and J. J. de Pablo, J. Chem. Phys. **102**, 2636 (1995).